Solute–solvent intermolecular vibronic coupling as manifested by the molecular near-field effect in resonance hyper-Raman scattering

Rintaro Shimada and Hiro-o Hamaguchi

Citation: The Journal of Chemical Physics **134**, 034516 (2011); doi: 10.1063/1.3512923
View online: http://dx.doi.org/10.1063/1.3512923
View Table of Contents: http://scitation.aip.org/content/aip/journal/jcp/134/3?ver=pdfcov
Published by the AIP Publishing

Solute–solvent intermolecular vibronic coupling as manifested by the molecular near-field effect in resonance hyper-Raman scattering

Rintaro Shimada[1] and Hiro-o Hamaguchi[1,2,a)]
[1]*Department of Chemistry, School of Science, The University of Tokyo, Hongo 7-3-1, Bunkyo, Tokyo 113-0033, Japan*
[2]*Institute of Molecular Science and Department of Applied Chemistry, National Chiao Tung University, 1001 Ta Hsueh Road, Hsinchu 300, Taiwan*

(Received 29 July 2010; accepted 18 October 2010; published online 21 January 2011)

Vibronic coupling within the excited electronic manifold of the solute all-*trans*-β-carotene through the vibrational motions of the solvent cyclohexane is shown to manifest as the "molecular near-field effect," in which the solvent hyper-Raman bands are subject to marked intensity enhancements under the presence of all-*trans*-β-carotene. The resonance hyper-Raman excitation profiles of the enhanced solvent bands exhibit similar peaks to those of the solute bands in the wavenumber region of 21 700–25 000 cm^{-1} (10 850–12 500 cm^{-1} in the hyper-Raman exciting wavenumber), where the solute all-*trans*-β-carotene shows a strong absorption assigned to the $1A_g \rightarrow 1B_u$ transition. This fact indicates that the solvent hyper-Raman bands gain their intensities through resonances with the electronic states of the solute. The observed excitation profiles are quantitatively analyzed and are successfully accounted for by an extended vibronic theory of resonance hyper-Raman scattering that incorporates the vibronic coupling within the excited electronic manifold of all-*trans*-β-carotene through the vibrational motions of cyclohexane. It is shown that the major resonance arises from the *B*-term (vibronic) coupling between the first excited vibrational level ($v = 1$) of the $1B_u$ state and the ground vibrational level ($v = 0$) of a nearby A_g state through ungerade vibrational modes of both the solute and the solvent molecules. The inversion symmetry of the solute all-*trans*-β-carotene is preserved, suggesting the weak perturbative nature of the solute–solvent interaction in the molecular near-field effect. The present study introduces a new concept, "intermolecular vibronic coupling," which may provide an experimentally accessible/theoretically tractable model for understanding weak solute–solvent interactions in liquid. © *2011 American Institute of Physics*. [doi:10.1063/1.3512923]

I. INTRODUCTION

Knowledge on solvent–solute interactions is essential for thorough understanding of chemical reactions in solution. Solvent molecules play various roles, such as being a reaction medium, giving/receiving energy as heat bath, promoting a reaction by stabilizing the intermediates, and triggering a reaction through the electrostatic interaction.[1–4] A single term "solvent effect" implicitly means a variety of perturbations imposed on a solute by surrounding solvent molecules. Unveiling the physical origin of the solvent effect at the molecular level is one of the major subjects of contemporary physical chemistry that still remain to be challenged. In order to understand the roles of solvents in the molecular language, we need a new method to selectively detect the solvent molecules in the vicinity of the solute and to discriminate them from those in the bulk.

Recently, we found a new phenomenon in resonance hyper-Raman (HR) scattering in solution, in which HR signal from the solvent was enhanced by more than five orders of magnitude.[5,6] HR spectra of all-*trans*-β-carotene in various solutions showed solvent dependent extra bands along with the bands assigned to all-*trans*-β-carotene itself. The peak positions of the additional bands accorded well with those of the strong infrared absorption bands of the solvents, although neat solvents did not exhibit any HR bands. An experiment with a deuteriated solvent showed expected deuteriation shifts of the extra HR bands. From these observations, we concluded that the extra HR bands originated from the solvents and that their intensities were enhanced by more than 5 orders of magnitude by the existence of all-*trans*-β-carotene, through a novel molecular phenomenon. We called this new phenomenon the "molecular near-field effect" in resonance HR scattering.[5] We developed an extended vibronic theory, which incorporated intermolecular coupling between the excited electronic states of all-*trans*-β-carotene, the solute, and the vibrations of the nearby solvent molecule to account for the observed enhancement.[6] We believe that this

a)Author to whom correspondence should be addressed. Electronic mail: hhama@chem.s.u-tokyo.ac.jp.

new phenomenon has a potential to provide a new spectroscopic tool that enables us to selectively, and directly, observe the solvent molecules existing in the close vicinity of the solute.

The purpose of the present paper is to elucidate, further, the mechanism of the solvent–solute interaction that facilitates the intensity enhancement of the solvent HR bands. In order to clarify the role of the solute electronic states in the enhanced solvent HR process, the excitation profiles of HR intensities of both the solute and the solvent are investigated. It is well known that the excitation profiles reflect sharply the resonance mechanism of HR scattering; they provide information on the locations and the symmetry of the resonant electronic states.[7–10] In the present study, the observed resonance HR excitation profiles of the solvent bands are compared with those of the solute. They are then quantitatively analyzed on the basis of our extended vibronic theory. The coupling mechanism and the assignments of the relevant electronic states are discussed. Detailed description of the molecular near-field effect, such as observed selection rules, solute dependence, and enhancement factors, has already been given in our previous paper.[6]

II. THEORY

The vibronic theory of resonance hyper-Raman scattering has been presented by a number of authors and is well established.[11–15] In order to account for the molecular near-field effect, we have extended the vibronic theory by explicitly introducing the solute–solvent interaction term in the form of intermolecular vibronic coupling.[6] The theory is briefly reviewed in the following.

The intensity of hyper-Raman transition from the initial state $|i\rangle$ to the final state $|f\rangle$ is proportional to the square of the first hyperpolarizability $(\beta_{\lambda\mu\nu})_{\mathrm{if}}$. An element of the first hyperpolarizability tensor $\beta_{\lambda\mu\nu}$ of a molecule with an excitation angular frequency ω_0 is expressed as follows[12,15,16]:

$$(\beta_{\lambda\mu\nu})_{if} \equiv \sum_n \sum_m \left[\frac{\langle f|\, R_\lambda\, |n\rangle \langle n|\, R_\mu\, |m\rangle \langle m|\, R_\nu\, |i\rangle}{(\varepsilon_m - \varepsilon_i - \hbar\omega_0)(\varepsilon_n - \varepsilon_i - 2\hbar\omega_0)} + \frac{\langle f|\, R_\nu\, |n\rangle \langle n|\, R_\lambda\, |m\rangle \langle m|\, R_\mu\, |i\rangle}{(\varepsilon_m - \varepsilon_i - \hbar\omega_0)(\varepsilon_n - \varepsilon_f + \hbar\omega_0)} + \frac{\langle f|\, R_\mu\, |n\rangle \langle n|\, R_\nu\, |m\rangle \langle m|\, R_\lambda\, |i\rangle}{(\varepsilon_n - \varepsilon_f + \hbar\omega_0)(\varepsilon_m - \varepsilon_f + 2\hbar\omega_0)} \right], \quad (1)$$

where ε_m, ε_n, ε_i, and ε_f represent the energies of the first and the second intermediate states $|m\rangle$, $|n\rangle$ and those of the initial $|i\rangle$ and final $|f\rangle$ states, respectively. Here, λ, μ, and ν refer to the polarization directions of the incident and scattered radiation fields in the molecular fixed frame.

When twice the energy of the incident photon is close to the transition energy of a molecular eigenstate, i.e., under a two-photon resonant condition, the contribution from the first term dominates in Eq. (1) and the latter two terms can be neglected.[16] Equation (1) then is rewritten as

$$(\beta_{\lambda\mu\nu})_{if} = \sum_m \frac{\langle f|\, R_\lambda\, |n\rangle \langle n|\, R_\mu\, |m\rangle \langle m|\, R_\nu\, |i\rangle}{(\varepsilon_m - \varepsilon_i - \hbar\omega_0)(\varepsilon_n - \varepsilon_i - 2\hbar\omega_0 - i\Gamma_{ni})}. \quad (2)$$

Here, Γ_{ni} is the damping constant. Under the Born–Oppenheimer approximation, the molecular eigenstates are expressed as products of pure electronic and pure vibrational eigenkets:

$$|i\rangle = |g]|i), \ |f\rangle = |g]|f), \quad |m\rangle = |m]|u), \text{ and } |n\rangle = |n]|v). \quad (3)$$

Only the hyper-Raman transition between the vibrational substates $|i)$ and $|f)$ of the ground electronic state $|g]$ is considered. $|\,]$ and $|)$ denote ket vectors in the pure electronic and pure vibrational spaces, respectively.[17] The adiabatic electronic kets are, further, expanded by the Herzberg–Teller expansion. Here, additional terms, which express the dependence of electronic kets on nuclear coordinates of nearby solvent molecule, are introduced to explicitly incorporate solute–solvent interactions. The Herzberg–Teller expansion for an arbitrary state $|s]$ is given as

$$|s] = |s^0] + \sum_a \sum_{e\neq s} |e^0] \frac{h^a_{es}}{(\varepsilon^0_s - \varepsilon^0_e)} Q^{\mathrm{solute}}_a + \sum_\alpha \sum_{e\neq s} |e^0] \frac{h^\alpha_{\mathrm{es}}}{(\varepsilon^0_s - \varepsilon^0_e)} Q^{\mathrm{solvent}}_\alpha + \cdots, \quad (4)$$

where

$$h^a_{es} = [e^0| \left(\frac{\partial H_{\mathrm{ev}}}{\partial Q^{\mathrm{solute}}_a} \right)_0 |s^0] \quad \text{and} \quad h^\alpha_{es} = [e^0| \left(\frac{\partial H_{\mathrm{ev}}}{\partial Q^{\mathrm{solvent}}_\alpha} \right)_0 |s^0].$$

$|e^0]$ and $|s^0]$ are the electronic eigenkets with energies ε^0_e and ε^0_s, respectively, under the crude adiabatic approximation where all the nuclear coordinates are fixed to the equilibrium positions. Here, H_{ev} is the Hamiltonian corresponding to the vibronic interaction energy, and Q^{solute}_a and $Q^{\mathrm{solvent}}_\alpha$ represent the normal coordinates of the solute and the proximate solvent molecule, respectively. The second term in Eq. (4) corresponds to the ordinary intramolecular vibronic coupling, whereas the third term the intermolecular vibronic coupling.

Substituting Eqs. (3) and (4) into Eq. (2) gives the hyperpolarizability expressed under the vibronic expansion. Rearranging terms in orders of their dependence on the nuclear coordinates and neglecting the second and higher-order terms, we obtain the following terms[6]:

$$
\begin{aligned}
&(\beta_{\lambda\mu\nu})_{if} = A + B_1 + B_1' + B_2 + B_2' \\
&A = \sum_{mu,v} F(\omega_0)(M_\lambda)_{gn}(M_\mu)_{nm}(M_\nu)_{mg}(f|v)(v|u)(u|i), \\
&B_1 = \sum_{\mathrm{mu},v}\sum_{a}\sum_{e\neq n} F(\omega_0)\left\{(M_\lambda)_{\mathrm{ge}}\, h^a_{\mathrm{en}}\left(M_\mu\right)_{\mathrm{nm}}(M_\nu)_{\mathrm{mg}}\frac{\left(f|\ Q_a^{\mathrm{solute}}|\ v\right)(v|\ u)(u|\ i)}{\varepsilon_n^0-\varepsilon_e^0}\right. \\
&\qquad \left. + (M_\lambda)_{\mathrm{gn}}\, h^a_{\mathrm{ne}}\left(M_\mu\right)_{\mathrm{em}}(M_\nu)_{\mathrm{mg}}\frac{(f|\ v)\left(v|\ Q_a^{\mathrm{solute}}|\ u\right)(u|\ i)}{\varepsilon_e^0-\varepsilon_n^0}\right\} \\
&B_1' = \sum_{\mathrm{mu},v}\sum_{\alpha}\sum_{e\neq n} F(\omega_0)\left\{(M_\lambda)_{\mathrm{ge}}\, h^\alpha_{\mathrm{en}}\left(M_\mu\right)_{\mathrm{nm}}(M_\nu)_{\mathrm{mg}}\frac{\left(f|\ Q_\alpha^{\mathrm{solvent}}|\ v\right)(v|\ u)(u|\ i)}{\varepsilon_n^0-\varepsilon_e^0}\right. \\
&\qquad \left. + (M_\lambda)_{\mathrm{gn}}\, h^\alpha_{\mathrm{ne}}\left(M_\mu\right)_{\mathrm{em}}(M_\nu)_{\mathrm{mg}}\frac{(f|\ v)\left(v|\ Q_\alpha^{\mathrm{solvent}}|\ u\right)(u|\ i)}{\varepsilon_e^0-\varepsilon_n^0}\right\}, \\
&B_2 = \sum_{\mathrm{mu},v}\sum_{a}\sum_{e\neq m} F(\omega_0)\left\{(M_\lambda)_{\mathrm{gn}}\left(M_\mu\right)_{\mathrm{ne}}\, h^a_{\mathrm{em}}(M_\nu)_{\mathrm{mg}}\frac{(f|\ v)\left(v|\ Q_a^{\mathrm{solute}}|\ u\right)(u|\ i)}{\varepsilon_m^0-\varepsilon_e^0}\right. \\
&\qquad \left. + (M_\lambda)_{\mathrm{gn}}\left(M_\mu\right)_{\mathrm{nm}}\, h^a_{\mathrm{me}}(M_\nu)_{\mathrm{eg}}\frac{(f|\ v)(v|\ u)\left(u|\ Q_a^{\mathrm{solute}}|\ i\right)}{\varepsilon_e^0-\varepsilon_m^0}\right\}, \\
&B_2' = \sum_{\mathrm{mu},v}\sum_{\alpha}\sum_{e\neq m} F(\omega_0)\left\{(M_\lambda)_{\mathrm{gn}}\left(M_\mu\right)_{\mathrm{ne}}\, h^\alpha_{\mathrm{em}}(M_\nu)_{\mathrm{mg}}\frac{(f|\ v)\left(v|\ Q_\alpha^{\mathrm{solvent}}|\ u\right)(u|\ i)}{\varepsilon_m^0-\varepsilon_e^0}\right. \\
&\qquad \left. + (M_\lambda)_{\mathrm{gn}}\left(M_\mu\right)_{\mathrm{nm}}\, h^\alpha_{\mathrm{me}}(M_\nu)_{\mathrm{eg}}\frac{(f|\ v)(v|\ u)\left(u|\ Q_\alpha^{\mathrm{solvent}}|\ i\right)}{\varepsilon_e^0-\varepsilon_m^0}\right\},
\end{aligned}
\tag{5}
$$

where

$$F(\omega_0) = \{(\varepsilon_{\mathrm{mu}} - \varepsilon_{\mathrm{gi}} - \hbar\omega_0)(\varepsilon_{\mathrm{nv}} - \varepsilon_{\mathrm{gi}} - 2\hbar\omega_0 - i\Gamma_{\mathrm{nv,gi}})\}^{-1}$$

and

$$(M_\lambda)_{\mathrm{nm}} = [n^0|R_\lambda|m^0].$$

A Herzberg–Teller expansion of the ground state is not considered in the present derivation. The A-term is the zeroth-order term, which gives the HR transition under the Condon approximation. The *B*-terms (B_1, B_1', B_2, and B_2') contain the first-order Herzberg–Teller coupling in the intermediate states and they correspond to Albrecht's *B*-term in linear resonance Raman scattering.[18] Subscripts 1 and 2 denote the vibronic coupling in the electronic state *n* and *m*, respectively, and the prime symbol (′) denotes the vibronic transition induced by the solvent normal coordinates.

The A-term is the leading term when a resonant electronic state *n* is simultaneously one- and two-photon allowed. On the other hand, the A-term vanishes for molecules possessing an inversion symmetry such as all-*trans*-β-carotene. The *B*-terms become major sources of the hyper-Raman intensities for such molecules. Each term in the *B*-terms can be decomposed into a product of one-photon and two-photon electronic transition moments and a vibronic coupling term that connects them. Therefore, both one- and two-photon allowed electronic states may equally contribute to the resonance enhancement. The B'-terms may give rise to solvent HR bands through the intermolecular vibronic coupling, $h^\alpha Q_\alpha^{\mathrm{solvent}}$, in the same manner as the ordinary intramolecular vibronic coupling; $h^a Q_a^{\mathrm{solute}}$, give rise to the solute resonance HR bands. Absolute magnitude of the intermolecular coupling constant, h^α, may be determined by the relative configuration of the solute and solvent molecules, the solvent vibrational modes and symmetries, etc. Though quantitative discussion of those factors is out of scope of this article, we can expect a resonance enhancement of the solvent modes by virtue of the solute excited electronic states. Measurements of the excitation profiles of the enhanced solvent bands will be a crucial test for the validity of our theory.

Note that the B_1- and B_1'-terms differ only by the origin of the normal coordinates, whether it is from the solute or the solvent. The electronic states are solely from the solutes, and the electronic transition moments and the resonant denominator have exactly the same expressions in both terms. Thus, notations on the normal coordinates indicating their origin will be omitted hereafter and general expression Q_a for the combined space of solute and solvent normal coordinates will be used in the following sections in order to avoid redundancy.

III. EXPERIMENTAL

Sample: All-*trans*-β-carotene and high-performance liquid chromatography grade cyclohexane were purchased from

Wako Chemical Corp. and used as received. The sample solution was prepared under deep red light in order to prevent the sample from undergoing photoisomerization. The concentration of the solution was 1 mM.

Apparatus: A wavelength tunable picosecond mode-locked Ti:sapphire oscillator (Spectra Physics, Tsunami) was used as the light source. The center wavelength of the output can be selected from 720 to 920 nm. The repetition rate and the typical pulse duration were 82 MHz and 3–4 ps, respectively. The output of the oscillator was attenuated by a neutral density filter and focused into a sample solution contained in a quartz fluorescence cuvette by a microscopic objective (x20; NA, 0.4). The scattered HR signal was collected in the back scattering geometry with the same objective and separated from the incident light by glass filters to be introduced into a polychromator (Horiba Jobin Yvon, iHR-320). Finally, the HR spectra were recorded on a liquid nitrogen cooled charge coupled device camera (Roper Scientific, Spec-10 2KB-EV/LN). Due to the nonlinearity of the HR process, the intensity of the HR scattering depends not only on the average power, but also on the pulse duration of the incident pulses. For the correction of any fluctuations of pulse characteristics during exposure, a fraction of the incident beam was separated and introduced into a β-barium borate crystal for second harmonic generation (SHG) and the intensity of SHG was simultaneously monitored during HR measurements. Wavelength dependence of the instrumental sensitivity was corrected.

Excitation profile measurement: The excitation wavelength was tuned from 800 to 920 nm (12 500 to 10 800 cm^{-1}) with 10 nm steps, and HR spectra of solution and neat solvent were measured at each wavelength. The pulse energy at the sample point was 0.6 nJ for the solution sample and 2.4 nJ for the neat solvent. The spectral distortion due to the self-absorption in the sample solution was corrected by assuming the Lambert–Beer's law and the Lorentzian shape depth profile[19] of the incident laser intensity. The correction procedure is as follows. A series of HR spectra were measured at different penetration depth of the focal spot in the sample solution. The observed HR intensity $I(\lambda, x)$ at each wavelength λ was plotted against the sample position x whose axis is along the optical axis. The obtained profiles were curve fitted by the equation below, which is a convolution of the squared laser intensity depth profile $L(x)^2$ with an exponential function $E(\lambda, x)$:

$$I(\lambda, x) = \int E(\lambda, x - t)\, L(t)^2 dt, \tag{6}$$

where

$$E(\lambda, x) = \begin{cases} I_0(\lambda) \exp[-\varepsilon(\lambda)\, ca\, (x - x_0)] \\ 0 \end{cases}$$

$$(x \geq x_0) \quad (x < x_0) \quad \text{and} \quad L(t) = \frac{N^{1/2}}{t^2 + w^2}.$$

Here c and $\varepsilon(\lambda)$ denote the sample concentration in mol L^{-1} and the molar extinction coefficient of β-carotene in cyclohexane, respectively, and measured values are used during the curve fitting. a is a correction factor for converting the sample position x to effective path length inside the sample solution in order to compensate for the refraction at air–cuvette interface. x_0 represents the position at the cuvette–sample interface. N and w are the normalization factor and the half width of the Lorentzian function, respectively, and $I_0(\lambda)$ is the original HR intensity at wavelength λ expected to be observed if there was no self-absorption effect. Observed $I(\lambda, x)$ is fitted by Eq. (6) with a, $I_0(\lambda)$, x_0, and w being parameters. The self-absorption corrected spectra $I_0(\lambda)$ were retrieved from the fitting parameter. This procedure is valid when HR scattering is emitted from small volume inside the sample solution with constant intensity. This is the case for our experiments because the HR signal only generates from the focal spot where the incident electromagnetic field is tightly focused by the microscopic objective and the sample solution has negligible absorption at laser fundamental wavelength.

The nonresonant HR bands of neat cyclohexane at 2933 cm^{-1} were measured under the same experimental condition, except for the magnified pulse energy by four times, at each excitation wavelength. They were used for external intensity standard when comparing HR intensities of different excitation wavelength. Broad background signal due to two-photon fluorescence was subtracted by fitting with a low order polynomial.

IV. RESULTS AND DISCUSSION

A. Excitation wavenumber dependent hyper-Raman spectra

Figure 1 shows the visible absorption spectrum of all-*trans*-β-carotene in cyclohexane. The vertical arrows in the figure indicate the two-photon wavenumbers of the 13 exciting lines used in the present experiment. Figure 2 shows the excitation wavenumber dependence of the resonance HR spectra of β-carotene in cyclohexane. While the excitation wavenumber is tuned from 12 500 cm^{-1} (800 nm) to 10 800 cm^{-1} (920 nm), where two-photon energy of the

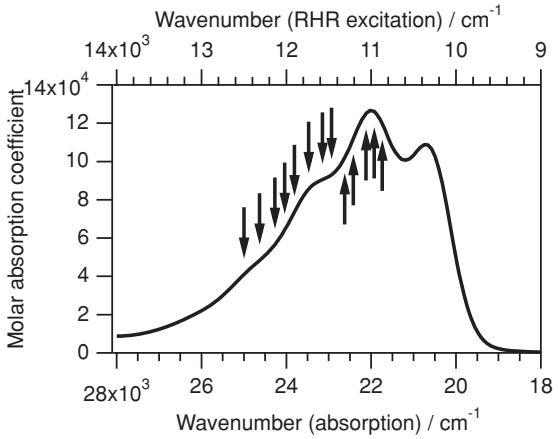

FIG. 1. Stationary absorption spectrum of β-carotene in cyclohexane. Arrows indicate the excitation wavenumber employed in the resonance hyper-Raman excitation profile measurement.

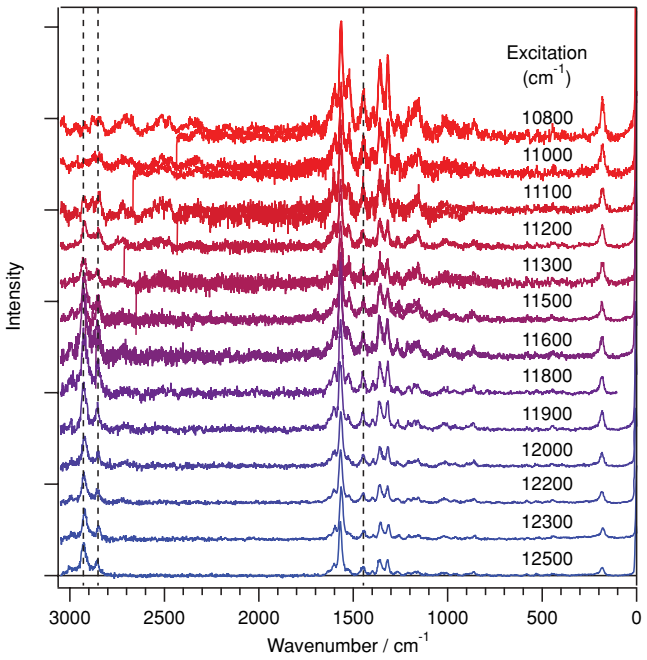

FIG. 2. Resonance hyper-Raman spectra of all-*trans*-β-carotene in cyclohexane excited from 12 500 to 10 800 cm^{-1} (800–920 nm). Excitation wavenumber of each spectrum is indicated in the figure. The vertical dotted lines indicate the enhanced bands of solvent, cyclohexane. The intensity normalization and the self-absorption correction of each spectrum have been done.

incident radiation overlaps with the blue side of the strongly allowed S_0 ($1A_g$) → S_2 ($1B_u$) absorption of β-carotene, several prominent bands are observed with varying intensities. Four HR bands at 1569, 1359, 1319, and 184 cm^{-1} are due to the vibrations of the solute all-*trans*-β-carotene. Three at 2933, 2857, and 1445 cm^{-1}, which are indicated by vertical dotted lines in Fig. 2, are assigned to the enhanced bands of the solvent, cyclohexane.[5,6] The peak positions of all the enhanced solvent band agreed with the bulk values within experimental uncertainties. The HR intensities of both the solute and the solvent gradually increase as the excitation wavelength is tuned toward the S_2 absorption maximum. We note that the lower signal to noise ratio in the lower excitation wavenumber is due to the interference from two-photon fluorescence whose peak lies around 18 900 cm^{-1}.

B. Excitation profiles

The intensity of each band in Fig. 2 is plotted against twice the wavenumber of the incident photon to present resonance hyper-Raman excitation profile (RHREP). Figure 3(a)–3(e) shows the RHREPs of the 1569 (a), 1319 (b), and 184 cm^{-1} (c) bands of the solute and the 2933 (d) and 1445 cm^{-1} (e) bands of the solvent. The one-photon absorption spectrum is also shown in each figure for comparison. All the RHREPs, including those of the solvent vibrations, show intensity enhancements as the two-photon wavenumber of the excitation photon falls into resonance with the S_2 absorption band of β-carotene. In fact, the RHREPs of the 1569 and 1319 cm^{-1} bands of β-carotene and the 1445 cm^{-1} bands of the solvent show almost identical profile with one another. This observation suggests that the enhanced solvent bands indeed gain its intensity through the electronic resonance with the excited state of the solute, as is predicted by our intermolecular vibronic coupling scheme. The next step is to identify the excited electronic states responsible for the enhancement. It is not obvious because β-carotene possesses several dark electronic states, namely $2A_g$ (S_1), $3A_g$, etc., near the strongly one-photon allowed $1B_u$ (S_2) state.[20–24] The $2A_g$ and the $3A_g$ states are not observable in the one-photon absorption spectrum. However, they are two-photon allowed and may contribute to the resonance hyper-Raman process through the two-photon resonance term.

C. 1–0 and 0–0 resonance

For the analysis of the excitation profiles, the sum over state expression, Eq. (5), is evaluated. Given the present experimental condition that the two-photon energy of the excitation radiation is overlapped with the absorption of the β-carotene molecule, the two-photon resonance condition is satisfied. Therefore, only the B_1- (and B_1'-) term in Eq. (5) is considered. Direct evaluation of the B_1-term is very complicated because many states are involved in the summation. Therefore, the following assumptions are introduced to further simplify the equation. First, the initial state is assumed to be the vibrational ground state ($v_a = 0$ where v_a is the vibrational quantum number of the mode a) of the ground electronic state. Second, the one-photon energy of the excitation radiation is much smaller than any molecular transition energies so that one-photon resonance denominator can be approximated as

$$\varepsilon_{\mathrm{mu}} - \varepsilon_{gi} - \hbar\omega_0 \sim \varepsilon_{m0} - \varepsilon_{\mathrm{gi}} - \hbar\omega_0.$$

Then, the sum over the vibrational states u can be closed to give following expression:

$$B_1 = \sum_{\mathrm{mv}'} \sum_{a} \sum_{e \neq n} \left(\varepsilon_{m0} - \varepsilon_{g0} - \hbar\omega_0\right)^{-1} \left\{ \frac{(M_\lambda)_{\mathrm{ge}}\, h^a_{\mathrm{en}}\, (M_\mu)_{\mathrm{nm}}\, (M_\nu)_{\mathrm{mg}}}{\left(\varepsilon_{n(0_a v')} - \varepsilon_{g0} - 2\hbar\omega_0 - i\Gamma_{n(0_a v'),g0}\right)} \frac{\left(1_a|\ Q_a|\ 0_a\right)\left(0_a|\ 0_a\right)}{\varepsilon^0_n - \varepsilon^0_e} \right.$$
$$\left. + \frac{(M_\lambda)_{\mathrm{gn}}\, h^a_{\mathrm{ne}}\, (M_\mu)_{\mathrm{em}}\, (M_\nu)_{\mathrm{mg}}}{\left(\varepsilon_{n(1_a v')} - \varepsilon_{g0} - 2\hbar\omega_0 - i\Gamma_{n(1_a v'),g0}\right)} \frac{\left(1_a|\ 1_a\right)\left(1_a|\ Q_a|\ 0_a\right)}{\varepsilon^0_e - \varepsilon^0_n} \right\} \left(f'|\ v'\right)\left(v'|\ 0'\right), \tag{7}$$

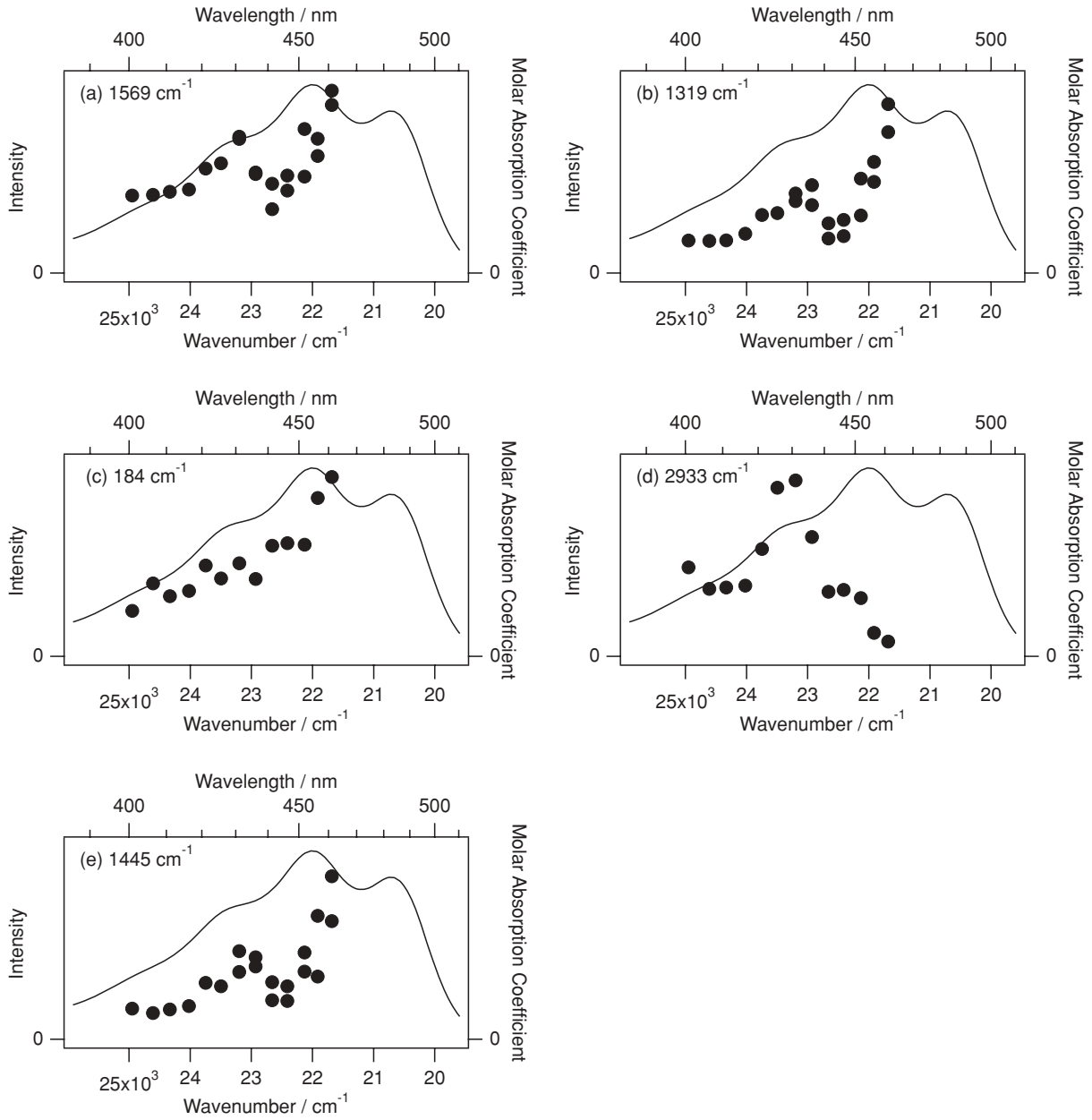

FIG. 3. Excitation profiles (•) of HR bands of solute at 1569 (a), 1319 (b), and 184 cm^{-1} (c) and those of solvent at 2933 (d) and 1445cm^{-1} (e). The solid line in each graph is the stationary one-photon absorption spectrum of β-caortene in cyclohexane.

where

$$|v) = |v_a)\,\big|v'\big) = |v_a) \prod_{i\neq a} |v_i)$$

and

$$\varepsilon_{n(v_a v')} = \varepsilon_{n0} + v_a \cdot \hbar\omega_a + \sum_{i\neq a} v_i \cdot \hbar\omega_i.$$

Here, $|v')$ represents a direct product of all the eigenkets in the nuclear coordinate space in the intermediate state n except for the mode Q_a that promotes the vibronic coupling. Equation (7) indicates that the B_1-term consists of two terms with different resonance behaviors. If the resonant excited state n is two-photon allowed but one-photon forbidden from the ground state, such as $2A_g$ or $3A_g$:

$$(M_\mu)_{\rm nm}(M_v)_{\rm mg} \neq 0 \quad \text{and} \quad (M_\lambda)_{\rm gn} = 0.$$

The second term vanishes and the first term solely contributes to the resonant enhancement. On the other hand, if the resonant state is one-photon allowed but two-photon forbidden,

$$(M_\lambda)_{\rm gn} \neq 0 \text{ and } (M_\mu)_{\rm nm}(M_v)_{\rm mg} = 0.$$

The first term vanishes and the second term will be the source of the hyper-Raman transition. Furthermore, the vibrational quantum number v_a of mode Q_a in the resonant electronic state n is 0 for the first term, whereas it is 1 for the second term. Therefore, the peak of the excitation profile coincides with the 0–0 band of the resonant electronic state (0–0 resonance) for the first term, while it coincides with the 1–0 band (1–0 resonance) for the second term. In both cases, the

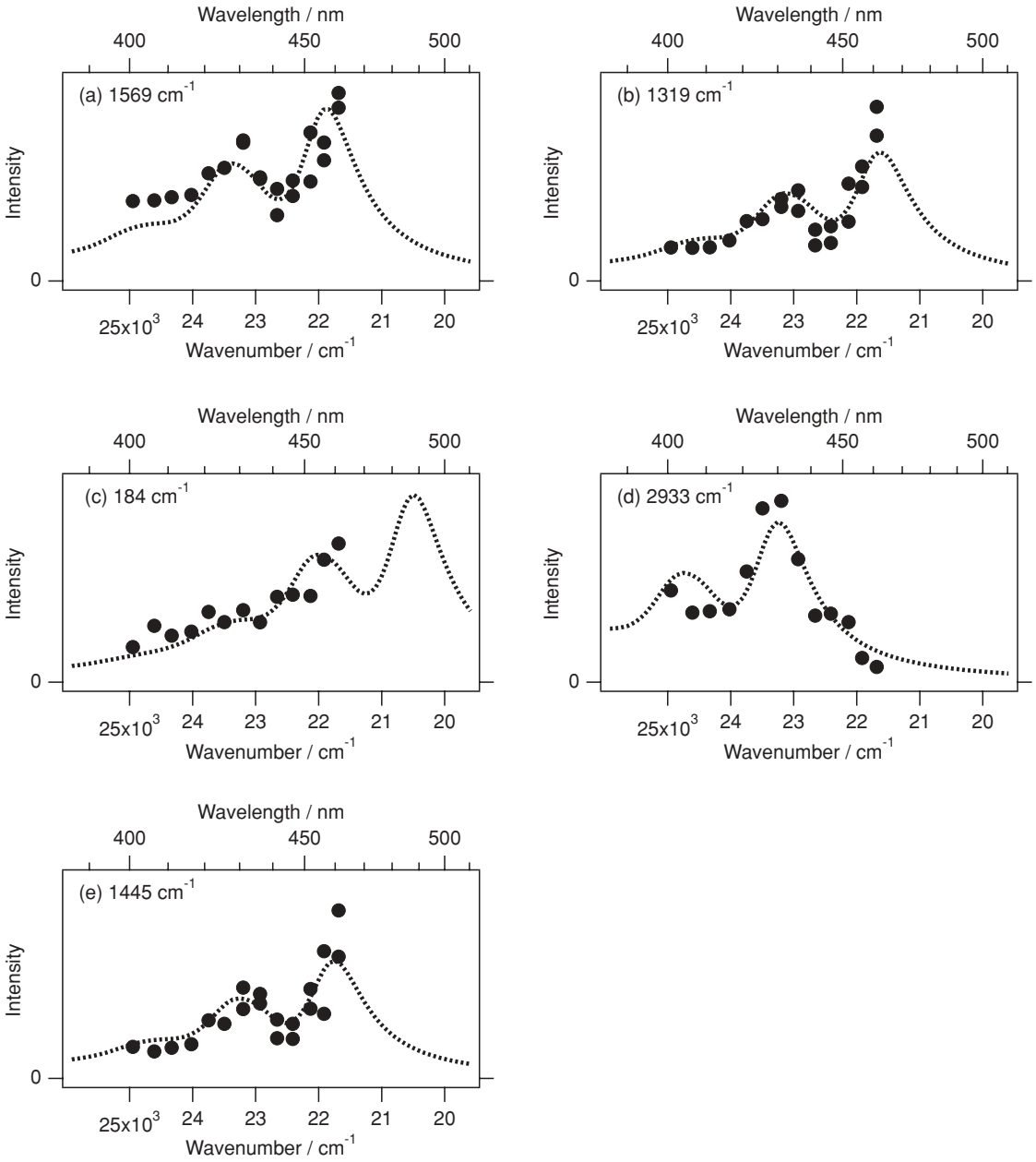

FIG. 4. Excitation profiles (•) of HR bands of solute at 1569 (a), 1319 (b), and 184 cm^{-1} (c) and those of solvent at 2933 (d) and 1445 cm^{-1} (e). The dotted lines are the simulated curves derived from the extended vibronic theory.

RHREPs may show progression of totally symmetric modes arising from the Franck–Condon (FC) factor. The FC factor may as well give rise to the combination bands between mode Q_a and the totally symmetric modes in hyper-Raman spectra, as Chung and Ziegler has pointed out.[11] This is analogous to the well-known *B*-term scattering mechanism in resonance Raman scattering.[17,18] In linear Raman scattering, one-photon allowed electronic states always facilitate both the 0–0 and the 1–0 resonances. In HR scattering, however, the 0–0 resonance can be observed only when excitation is resonant with the two-photon allowed state, while the 1–0 resonance with the one-photon state. It is possible to know the symmetry of the resonant electronic state by the peak positions of the RHREPs.

D. Simulation of the excitation profiles

RHREPs in Fig. 3 show clear dependence of the peak positions on vibrational modes, indicating that the enhancement arises from the 1–0 resonance with the $1B_u$ state. The two low lying A_g states, $2A_g$ and $3A_g$, can be the vibronic coupling counterpart of $1B_u$. We argue that the $3A_g$ (0–0 transition wavenumber 18 000—25 000 cm^{-1}) (Refs. 21, 24, and 25) is more likely than $2A_g$ (0–0 transition wavenumber ~14 500 cm^{-1}) (Ref. 24) because of the smaller energy gap from the $1B_u$ state (20 800 cm^{-1}). Then, the 0–0 resonance with $3A_g$ is expected as well as the 1–0 resonance with $1B_u$. However, the $3A_g$ resonance is not obvious in the observed RHREPs in Fig. 4. We note the

TABLE I. Parameters obtained from the curve fitting of RHREPs.

Δ_1[a]	Δ_2[a]	Δ_3[a]	ν_1[a] / cm^{-1}	ν_2[a] / cm^{-1}	ν_3[a] / cm^{-1}	ν_{n0}[b] / cm^{-1}	σ[c] / cm^{-1}	Solvent	Temperature /K	Reference
0.99	0.73	0.56	1525	1125	1005	20 400	560[d]	Cyclohexane	298	This work
1.06	0.93	0.59	1525	1155	1005	20 800	450[d], 80[e]	*n*.Hexane	298	Ref. 28
1.2	0.9	0.7	1525	1155	1005	20 950	450[d], 80[e]	Isopentane	298	Ref. 32
1.17	0.70	0.46	1523	1155	1006	20 150	280[d], 80[e]	Isopentane	10	Ref. 31

[a]Δ_i, and ν_i represent the displacement parameters and the frequencies (in cm^{-1}) of ν_1, ν_2, and ν_3, the three prominent totally symmetric modes of all-*trans*-β-carotene, respectively.
[b]The 0–0 energy (in cm^{-1}) of the $1B_u$ (S_2) electronic state.
[c]The damping constant for the $1B_u$ (S_2) electronic state.
[d]Homogeneous width.
[e]Inhomogeneous width.

following two possibilities to account for this absence of the $3A_g$ resonance peak. One is that the $3A_g$ state is not located in the two-photon excitation wavenumber range (21 700–25 000 cm^{-1}) presently studied. The other is that the damping constant for the $1A_g \rightarrow 3A_g$ transition is very large so that the resonance with the $3A_g$ state is too broad to be observed as a clear peak in the excitation profiles. Measurements of RHREPs for a wider excitation wavenumber range will be necessary to elucidate the effect of the $3A_g$ resonance.

Simulations of the excitation profiles based on the sum over state expression Eq. (7) is made. In order to reduce the computational complexities, further assumptions in the following are made: (i) Resonant state is $1B_u$ and only the 1–0 resonance term is considered; (ii) Vibrational frequencies in the $1B_u$ states are the same as those in the ground states; (iii) Harmonic vibrational wavefunctions are used; (iv) For the calculation of the FC factors, only the three totally symmetric ν_1, ν_2, and ν_3 modes of all-*trans*-β-carotene, which give rise to the prominent three bands in resonance Raman scattering,[26,27] are taken into consideration up to the combined quantum number of 4; (v) Only the homogeneous broadening contribution to the damping is considered. Although the assumption (ii) does not always hold in general, many reports on the Raman excitation profiles of β-carotene show the similarity of frequencies in the $1B_u$ states to those in the ground state.[28–30]

Figures 4(a)–4(e) show the simulated curves derived from Eq. (7) that reproduce the experimental results the best. Table I summarizes the parameters obtained from the fitting together with the values reported in the literature[28,31,32] from the resonance Raman experiments. Although the model employed in the present analysis takes into account the resonance with $1B_u$ state only, the observed RHREPs as well as the progressions due to totally symmetric modes are well reproduced by the simulation. The obtained parameters are also in good agreement with the literature. It should be emphasized that the RHREPs of the solvent are well simulated by Eq. (7), indicating the molecular near-field effect originates from the intermolecular vibronic coupling mechanism.

Appearance of new peaks above 2000 cm^{-1} by the excitation at 11 200 cm^{-1} and lower wavenumber light is also well accounted for by Eq. (7). Figure 5 shows the HR spectra of β-carotene with the excitation at 11 100 cm^{-1}. As discussed in Sec. IV C, the FC terms may give rise to the additional combination bands of totally symmetric modes and the HR active fundamentals. In fact, most bands in the Fig. 5 are successfully assigned to the combinations as indicated in the figure.

Finally, we discuss the nature of the solute–solvent interaction that facilitates the intermolecular vibronic coupling. The term "intermolecular vibronic coupling" is not entirely new if intermolecular interactions within stable molecular complexes,[33–35] aggregates,[36–38] or crystals[39,40] are discussed. For such systems, intermolecular interactions are strong in the ground electronic states so that symmetry lowering and changes in the electronic structures accompany. Intermolecular vibronic coupling in these molecular complexes is a consequence of such strong interactions. However, the new solute–solvent interaction found in the present study does not require such strong interaction in the electronic ground state. The observed HR spectra and the excitation profiles for the molecular near-field effect are well explained under the framework of vibronic (*B*-term) resonance scheme, which becomes the leading term only when the system retains the inversion symmetry and is not structurally distorted. It indicates that the symmetry and the property in the electronic states of the solute molecule are preserved at the zeroth order and that the intermolecular interaction acts only as a weak first-order perturbation in the excited electronic manifold, where two closely lying B_u and A_g states are coupled by the vibrations of the proximate solvent molecule. The coupled

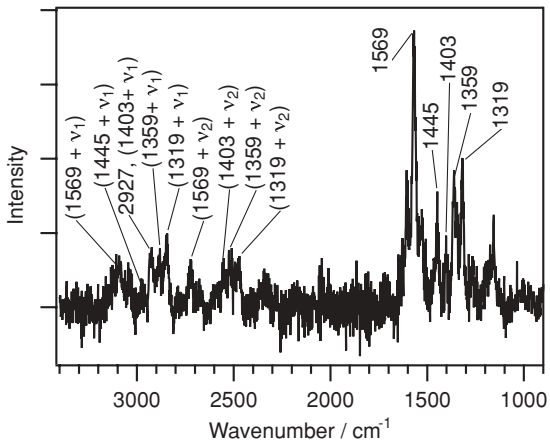

FIG. 5. Hyper-Raman spectrum of all-*trans*-β-carotene in cyclohexane excited at 11 100 cm^{-1}. The combination bands between the HR active fundamentals and the Franck–Condon active ν_1 (1525 cm^{-1}) or ν_2 (1155 cm^{-1}) modes are observed.

solute–solvent system may have structure and lifetime that dynamically vary. Such weak and dynamic solute–solvent interaction is often referred to as solvation effects in liquid media. Further investigation of the intermolecular vibronic coupling mechanism will lead to deeper understanding of the microscopic nature of solvation.

V. CONCLUSION

The excitation profiles of the molecular near-field effect in resonance hyper-Raman scattering are studied. The observed spectra and the excitation profiles are well accounted for by the extended vibronic theory of resonance hyper-Raman scattering. The RHREPs observed in the present work unequivocally showed the existence of coupling between the solute electronic states with the neighboring solvent vibrations, namely the intermolecular vibronic coupling. Further analysis of intensity and otherwise unobtainable, peak position, band shape, and the selection rules of the enhanced band will provide valuable information of the solvent molecule in the vicinity of solute.

ACKNOWLEDGMENTS

This research has been supported by a Grant-in-Aid for Young Scientists (B) to R.S. (Grant No. 22750008) from the Ministry of Education, Culture, Sports, Science, and Technology of Japan.

[1]A. Marcus and N. Sutin, Biochim. Biophys. Acta **811**, 265 (1985).
[2]D. Borgis and J. T. Hynes, J. Chem. Phys. **94**, 3619 (1991).
[3]R. M. Stratt, Acc. Chem. Res. **28**, 201 (1995).
[4]M. W. Wong, M. J. Frisch, and K. B. Wiberg, J. Am. Chem. Soc. **113**, 4776 (1991).
[5]R. Shimada, H. Kano, and H. Hamaguchi, J. Raman Spectrosc. **37**, 469 (2006).
[6]R. Shimada, H. Kano, and H. Hamaguchi, J. Chem. Phys. **129**, 024505 (2008).
[7]L. C. T. Shoute, G. P. Bartholomew, G. C. Bazan, and A. M. Kelley, J. Chem. Phys. **122**, 184508 (2005).
[8]A. M. Kelley, J. Phys. Chem. A **112**, 11975 (2008).
[9]Y. C. Chung and L. D. Ziegler, J. Chem. Phys. **89**, 4692 (1988).
[10]M. Mizuno, H. Hamaguchi, and T. Tahara, J. Phys. Chem. A **106**, 3599 (2002).
[11]Y. C. Chung and L. D. Ziegler, J. Chem. Phys. **88**, 7287 (1988).
[12]L. D. Ziegler, J. Raman Spectrosc. **21**, 769 (1990).
[13]A. M. Kelley, Annu. Rev. Phys. Chem. **61**, 41 (2010).
[14]V. I. Petrov, Opt. Spectrosc. **59**, 788 (1985).
[15]J. P. Neddersen, S. A. Mounter, J. M. Bostick, and C. K. Johnson, J. Chem. Phys. **90**, 4719 (1989).
[16]D. A. Long and L. Stanton, Proc. R. Soc. London, Ser. A **318**, 441 (1970).
[17]H. Hamaguchi, in *Advances in Infrared and Raman Spectroscopy*, edited by R. J. H. Clark and R. E. Hester (Wiley, New York, 1985), Vol. 12, p. 273.
[18]C. Albrecht, J. Chem. Phys. **34**, 1476 (1961).
[19]C. J. De Grauw, N. M. Sijtsema, C. Otto, and J. Greve, J. Microsc. **188**, 273 (1997).
[20]R. J. Thrash, H. L. B. Fang, and G. E. Leroi, J. Chem. Phys. **67**, 5930 (1977).
[21]T. Polívka and V. Sundström, Chem. Phys. Lett. **477**, 1 (2009).
[22]H. Hashimoto, K. Yanagi, M. Yoshizawa, D. Polli, G. Cerullo, G. Lanzani, S. De Silvestri, A. T. Gardiner, and R. J. Cogdell, Arch. Biochem. Biophys. **430**, 61 (2004).
[23]P. Tavan and K. Schuten, Phys. Rev. B **36**, 4337 (1987).
[24]T. Polívka and V. Sundström, Chem. Rev. **104**, 2021 (2004).
[25]E. Ostroumov, M. G. Müller, C. M. Marian, M. Kleinschmidt, and A. R. Holzwarth, Phys. Rev. Lett. **103**, 108302 (2009).
[26]S. Saito, M. Tasumi, and C. H. Eugster, J. Raman Spectrosc. **14**, 299 (1983).
[27]F. Inagaki, M. Tasumi, and T. Miyazawa, J. Mol. Spectrosc. **50**, 286 (1974).
[28]W. Siebrand and M. Z. Zgierski, J. Chem. Phys. **71**, 3561 (1979).
[29]L. C. Hoskins, J. Chem. Phys. **72**, 4487 (1980).
[30]H. Torii and M. Tasumi, J. Phys. Chem. **94**, 227 (1990).
[31]A. R. Mantini, M. P. Marzocchi, and G. Smulevich, J. Chem. Phys. **91**, 85 (1989).
[32]Z. Z. Ho, R. C. Hanson, and S. H. Lin, J. Chem. Phys. **77**, 3414 (1982).
[33]M. Stavola, L. Isganitis, and M. G. Sceats, J. Chem. Phys. **74**, 4228 (1981).
[34]R. L. Fulton and M. Gouterman, J. Chem. Phys. **41**, 2280 (1964).
[35]A. Pakhomov, S. Ekbundit, C. Huie Lin, R. G. Alden, and S. H. Lin, J. Lumin. **63**, 129 (1995).
[36]P. Hildebrandt, M. Tsuboi, and T. G. Spiro, J. Phys. Chem. **94**, 2274 (1990).
[37]D. L. Akins and H.-R. Zhu, Langmuir **8**, 546 (1992).
[38]A. J. Fleming, J. N. Coleman, A. B. Dalton, A. Fechtenkötter, M. D. Watson, K. Müllen, H. J. Byrene, and W. J. Blau, J. Phys. Chem. B **107**, 37 (2003).
[39]J. Gierschner, M. Ehni, H.-J. Egelhaaf, B. M. Medina, D. Beljonne, H. Benmansour, and G. C. Bazan, J. Chem. Phys. **123**, 144914 (2005).
[40]J. Gierschener, H.-G. Mack, D. Oelkrug, I. Waldner, and H. Rau, J. Phys. Chem. A **108**, 257 (2004).